



## Article

# Spatiotemporal Distribution of Drought Based on the Standardized Precipitation Index and Cloud Models in the Haihe Plain, China

Yujuan Fu <sup>1</sup>, Xudong Zhang <sup>1,\*</sup> , Ray G. Anderson <sup>2,3</sup> , Ruiqiang Shi <sup>1</sup>, Di Wu <sup>4</sup> and Qiucheng Ge <sup>1</sup>

<sup>1</sup> College of Water Conservancy, Shenyang Agricultural University, Shenyang 110866, China; fyj0249@syau.edu.cn (Y.F.); srq0514@163.com (R.S.); 13842329260@163.com (Q.G.)

<sup>2</sup> USDA-Agricultural Research Service, US Salinity Laboratory, Riverside, CA 92501, USA; ray.anderson@usda.gov

<sup>3</sup> Department of Environmental Sciences, University of California-Riverside, Riverside, CA 92521, USA

<sup>4</sup> Irrigation and Drainage Development Center, Beijing 100054, China; wudisyau075@163.com

\* Correspondence: zxxddd@syau.edu.cn

**Abstract:** The Haihe Plain is the largest component of the agriculturally vital North China Plain, and it is characterized by serious water shortage and frequent droughts, which lead to crop reduction and have adverse effects on agriculture and ecology. We used daily precipitation data from 1955–2017; the region's spatiotemporal characteristics of drought were analyzed by using the standardized precipitation index (SPI), drought probability, and Mann–Kendall test for seasonal scale including two main crops growth seasons for the region's main crops. Furthermore, a cloud algorithm model was established to analyze the dispersion and instability of the SPI. The annual drought frequency is 28.57%; the SPI for spring has an increasing tendency, while summer shows a significant decreasing trend ( $p < 0.05$ ); the Haihe Plain has had a tendency towards drought over the last 63 years. The SPI in northwest is the smallest and increases gradually toward the south; the severity of drought in dry years increased from southeast to northwest. The cloud model shows that the SPI randomness of each site decreased significantly and tended to be stable and uniform. The deterministic and stable SPI of each station is stronger in dry years, and the randomness and instability are stronger in wet years. The inter-annual differences of the characteristic values of the SPI cloud model are bigger than the differences among sites, and the inter-annual randomness and inhomogeneity of the SPI are higher.

**Keywords:** standardized precipitation index; spatiotemporal characteristics; cloud model; homogeneity and stability; Mann-Kendall test



**Citation:** Fu, Y.; Zhang, X.; Anderson, R.G.; Shi, R.; Wu, D.; Ge, Q.

Spatiotemporal Distribution of Drought Based on the Standardized Precipitation Index and Cloud Models in the Haihe Plain, China.

*Water* **2022**, *14*, 1672. <https://doi.org/10.3390/w14111672>

Academic Editors: Yared Bayissa, Assefa M. Melesse and Tsegaye Tadesse

Received: 12 April 2022

Accepted: 20 May 2022

Published: 24 May 2022

**Publisher's Note:** MDPI stays neutral with regard to jurisdictional claims in published maps and institutional affiliations.



**Copyright:** © 2022 by the authors. Licensee MDPI, Basel, Switzerland. This article is an open access article distributed under the terms and conditions of the Creative Commons Attribution (CC BY) license (<https://creativecommons.org/licenses/by/4.0/>).

## 1. Introduction

Drought is one of the major causes of agricultural yield losses globally and in China. Due to global warming, extreme drought events have increased in recent years and generated profound socio-economic and environmental impacts [1–3]. Of the total area affected by various meteorological disasters, drought accounts for 60%. In China, the average area of cultivated land that is affected by drought is  $2.07 \times 10^7$  ha, and approximately  $1.0 \times 10^{10}$  kg of grain is lost due to drought every year [3,4]. The Haihe River Catchment is one of the seven biggest catchments in China. It is important because of the fact that two mega cities, Beijing and Tianjin, are located in the catchment. With the rapid development of agriculture, local economy, and population, the area has changed from a once dominant flood plain to a drought plain with acute water shortages exacerbated by quick declines of surface and sub-surface water levels [5].

Several studies have assessed the potential impact of climate change using different indicators depending on drought types [6]. Precipitation is the most common variable used in such studies, and it is frequently used in combination with other variables such as

temperature and soil moisture. In the 1960s, the Palmer Drought Severity Index (PDSI) was proposed as a drought index, which considered precipitation, temperature, soil moisture, evapotranspiration, and other factors. The PDSI, modified PDSI, Palmer Hydrological Drought Index (PHDI), and Z Index have all been used in previous drought research [7,8]. In the 1990s, the standardized precipitation index (SPI) was proposed by McKee et al. [1]. The SPI is based on the precipitation record and was first fitted to a probability distribution, then transformed through an equal-probability transformation into a normal distribution. This standardization ensures that SPI values can be compared across different locations. Moreover, SPI can be calculated at different timescales, ranging from 1 month to several years. This index is promoted by the World Meteorological Organization for global applications because it is simple to calculate, has multiple timescales, and can be applied in most places of the world. Based on SPI, the standardized precipitation evapotranspiration index (SPEI) was proposed afterward, which also considers potential evapotranspiration [9,10]. By calculating the difference between these two indexes, the characteristics of drought and flood variation can be objectively obtained.

Because of its simple and probabilistic nature, the SPI was recommended as the primary drought index for agricultural applications [11]. In 1996, Hayes et al., used the SPI to monitor a severe drought in the Southern Great Plains in the southwestern United States [12]. In this study, the SPI identified the drought onset and severity 1 month in advance of the PDSI. Lloyd-Hughes and Saunders [13] compared the abilities of the SPI and PDSI in monitoring droughts and concluded that the SPI provided a more appropriate spatial standardization. Following this serial comparison, the SPI has been widely used in drought event analysis [2], drought risk analysis [14], and to analyze the spatiotemporal variation characteristics of drought in different regions [3,15,16].

In practice, as drought is a dynamic cognitive process influenced by many factors, uncertainties often exist in a more complex, composite format. The SPI has considerable uncertainty because it is derived from precipitation. To quantify this uncertainty, the cloud model can be used; this model was put forth by Li et al. [17]. It is based on the uncertainty (randomness and fuzziness) of a human-defined concept and describes the connotation of an uncertain concept quantitatively through three digital characteristics [18]: *Ex* (Expectation), *En* (Entropy), and *He* (Hyper-Entropy). To date, the cloud model has been widely applied in many aspects, solving decision-making programs associated with various uncertainties [19–23], evaluation of water resources' carrying capacity [24], or classification and clustering [25,26]. It is also applied in the research of spatiotemporal distribution of random variables in many places in China. Yin et al. [27] used a cloud model to analyze the spatiotemporal distribution characteristics of reference crop evapotranspiration in Gansu Province, China. Cheng et al. [28] used the Z index and cloud model to analyze the drought characteristics of 22 meteorological stations in the hills of central Sichuan, China for a 60-year period. Long et al. [29] used the relative humidity index and cloud model to analyze the drought characteristics of eight meteorological stations in the hills of central Sichuan for a 51-year period. Jin et al. [30] analyzed the drought characteristics of 14 meteorological stations in Anhui Province, China for a period of 51 years by using the precipitation anomaly percentage and cloud model. The application of the cloud model in the analysis of the spatial characteristics of the eigenvalues, especially in the study of the spatiotemporal distribution of drought, shows that the method is effective for studying the spatiotemporal uniformity and stability of droughts.

While there has been extensive work on both the SPI and cloud models in China, there has not been work on applying these approaches to the Haihe Plain, which is a critical agricultural region of China, and which is both susceptible to drought and experiencing current water overuse. In this study, we calculated the spatiotemporal distribution characteristics of SPI at a seasonal scale across the Haihe Plain to analyze the temporal and spatial distribution trends of drought. We used the cloud model to understand the uniformity and stability of the drought. The results are expected to provide a reference for water resource

management, drought resistance, and ecological protection in the Haihe region of the North China Plain.

## 2. Materials and Methods

### 2.1. Study Area

The Haihe Plain is located in the north portion of the North China Plain and is the main agricultural area in the region. It includes Beijing and Tianjin cities, and Hebei, Shandong, and Henan provinces (Figure 1). The region covers an area of approximately  $12.8 \times 10^5$  km<sup>2</sup>, with an altitude ranging from ~100 m above sea level (in Shijiazhuang) to approximately 3 m (along the Bohai Sea). With a high population density and frequent double cropping cultivation practices with supplemental irrigation, this area experiences the most serious water shortage in China. The Haihe Plain has a warm humid or semi-humid climate. The spring is dry with little rain and has strong evaporation. The summer is rainy and the winter is dry and cold. The annual average precipitation is 400–700 mm, and seasonal drought is a typical occurrence [31].

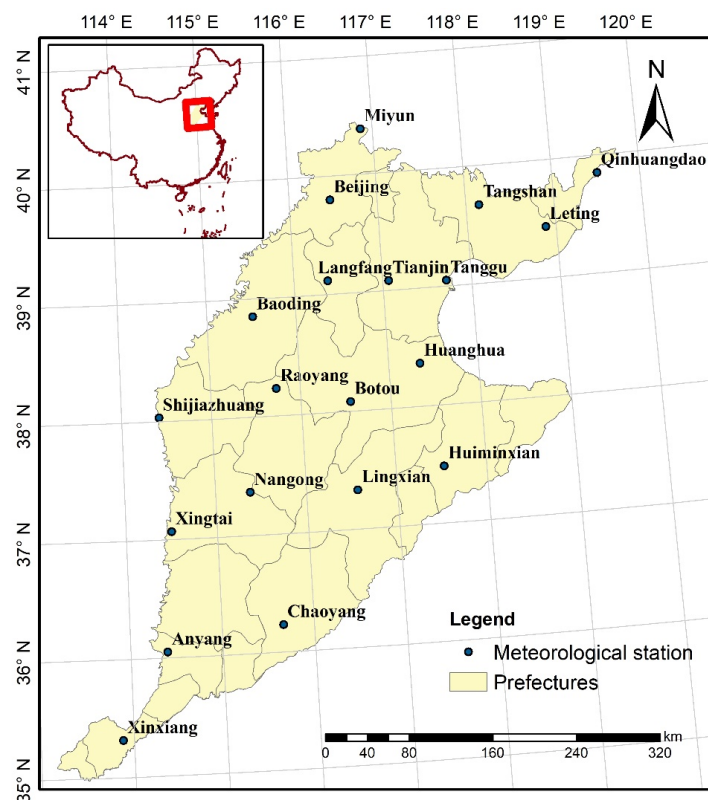


**Figure 1.** Location of the Haihe Plain within China and the distribution of weather stations.

### 2.2. Data Acquisition

The data used for this study were daily precipitation data from 1955 to 2017 from 20 basic meteorological stations in the Haihe Plain (Figure 1). These data were obtained from the Chinese Meteorological Science Data Sharing Service Network (<http://data.cma.cn>; accessed on 25 June 2020). After a consistency test and missing data processing, the dataset could be used as the calculation basis of the SPI [32].

According to the general division of meteorology and the climatic characteristics of the Haihe Plain, the corresponding periods of each season are spring (March–May), summer (June–August), autumn (September–November), and winter (December–February). Summer maize in the Haihe Plain is usually sown in the middle of June and harvested in late September; therefore, the growth period of maize (MGP) is from June to September. Wheat

is generally sown in October and matures at the end of May of the following year, thus, the growth period of wheat (WGP) extends from October to May of the following year.

2.3. Methods

2.3.1. Standardized Precipitation Index (SPI)

In SPI calculations, it is assumed that precipitation variability in a sequence follows a gamma distribution [33]. After processing the distribution probability of precipitation through normal standardization, a standardized cumulative frequency distribution for precipitation can be applied to classify drought levels. The SPI is computed as follows in Equation (1) [32,33]:

$$SPI = s \frac{t - (c_2t + c_1)t + c_0}{[(d_3t + d_2)t + d_1]t + 1.0} \tag{1}$$

where  $t = (\ln((1 - H(x))^{-2}))^{1/2}$  when  $H(x) > 0.5$  and  $t = (\ln(H(x)^{-2}))^{1/2}$  when  $H(x) \leq 0.5$ ,  $H(x) = q + (1 - q) G(x)$ ;  $q$  is the probability of zero,  $x$  is the precipitation (mm);  $G(x)$  is the cumulative probability of a given timescale;  $s$  is the positive and negative coefficient of probability density, when  $H(x) > 0.5$  and  $s = 1$ , and when  $H(x) \leq 0.5$ ,  $s = -1$ ,  $c_0 = 2.515517$ ,  $c_1 = 0.802853$ ,  $c_2 = 0.010328$ ,  $d_1 = 1.432788$ ,  $d_2 = 0.189269$ , and  $d_3 = 0.001308$  [33,34].

In China, SPI can be classified by the nine grades of meteorological drought of China as shown in Table 1 [35]. While SPI is frequently calculated on a seasonal to annual basis on different intervals [9], we chose to calculate the SPI of the Haihe Plain on both a seasonal (spring, summer, autumn, and winter), annual, and cropping season (MGP and WGP) basis.

**Table 1.** SPI and drought classifications according to the Chinese meteorological grading system.

Category	Extreme Wet	Severe Wet	Moderate Wet	Slight Wet	Near Normal	Slight Drought	Moderate Drought	Severe Drought	Extreme Drought
SPI	[2, ∞)	[1.5, 2)	[1.0, 1.5)	[0.5, 1.0)	(−0.5, 0.5)	(−1.0, −0.5]	(−1.5, −1.0]	(−2.0, −1.5]	(−∞, −2.0]

The SPIs over different timescales in Haihe Plain were calculated using the average regional precipitation based on the Tyson polygon.

2.3.2. Drought Frequency

Drought frequency [36] is represented by number of drought years and the total number of years Equation (2). We calculated the drought frequency of each station by different timescales and different drought grades as shown in Equation (2):

$$DF_{i,j} = \frac{n_{i,j}}{N} \tag{2}$$

where  $DF_{i,j}$  is the drought frequency of the meteorological station;  $i$  represents the drought grade (slight, moderate, severe, and extreme);  $j$  represents the timescales (spring, summer, autumn, winter, MGP, WGP, and annual);  $n_{i,j}$  is the number of years in the  $i$ th drought grade of the  $j$ th timescales; and  $N$  is the total number of years ( $N = 63$ ).

2.3.3. Mann-Kendall (MK) Trend Test

An investigation of different timescales series and trend analysis was performed for the entire area. One of the commonly used non-parametric trend tests in climatic and hydrologic time series is the Mann–Kendall (MK) trend test [37]. It has some advantages such as it does not require normally distributed data and the sensitivity of the test result is very low [38,39]. The MK trend analysis was applied to the SPI to investigate the trend changes over many regions of the world [40–42]. It searches for a trend in a series without specifying whether the trend is linear or nonlinear. Given a time series  $x(t)$  with a length of

$n$ , the null hypothesis of no trend assumes that  $x(t)$  is independently distributed. The MK test is based on the test statistic  $S$ , which is defined according to Equation (3) as:

$$S = \sum_{i=2}^n \sum_{j=1}^{i-1} \text{sgn}(X_i - X_j) \tag{3}$$

in which Equation (4),

$$\begin{cases} \text{sgn}(x) = 1 & x > 0 \\ \text{sgn}(0) = 0 & x = 0 \\ \text{sgn}(x) = -1 & x < 0 \end{cases} \tag{4}$$

A positive (negative) value of  $S$  indicates an upward (downward) trend. The statistic  $S$  is approximately normally distributed when  $n > 8$ , with the variance  $\text{Var}(S)$  as follows in Equation (5):

$$\text{Var}(S) = \frac{n(n-1)(2n+5)}{18} \tag{5}$$

The standardized test statistic  $Z$  follows the standard normal distribution Equation (6):

$$\begin{cases} Z = \frac{S-1}{\sqrt{\text{var}(S)}} & S > 0 \\ Z = 0 & S = 0 \\ Z = \frac{S+1}{\sqrt{\text{var}(S)}} & S < 0 \end{cases} \tag{6}$$

The corresponding  $p$ -value ( $p$ ) for the one-tailed test is respectively given by Equation (7):

$$p = 0.5 - \Phi(|Z|) \tag{7}$$

$$\Phi(|Z|) = \frac{1}{\sqrt{2\pi}} \int_0^{|Z|} e^{-t^2/2} dt$$

If the  $p$ -value is small enough, the trend is quite unlikely to be caused by random sampling. The trend is decreasing if  $Z$  is negative and increasing if  $Z$  is positive. At the significance level of 0.05, if  $p \leq 0.05$ , then the existing trend is considered to be statistically significant.

The Sen’s slope was used to determine the magnitude of the trends after obtaining the direction of the trend with the MK test. A linear model was used to calculate the change of slope [43] as shown in Equations (8) and (9):

$$Q_i = \frac{(X_j - X_k)}{(j - k)} \text{ for all } k < j \text{ and } i = 1, \dots, N \tag{8}$$

$$Q_{med} = \begin{cases} Q\left[\frac{(N+1)}{2}\right] & \text{where } N \text{ is odd} \\ Q\left(\frac{N}{2}\right) + Q\left[\frac{(N+2)}{2}\right], & \text{where } N \text{ is even} \end{cases} \tag{9}$$

where  $Q_i$  is the slope between data points  $X_j$  and  $X_k$ , and  $Q_{med}$  is Sen’s slope estimator, which reflects the direction of the trend in the data. All the statistical calculations for the  $Z$ ,  $p$  value, and Sen’s slope of SPI for the seven timescales were conducted using Burkey’s code [44] in Matlab.

### 2.3.4. Cloud Model

Cloud model is a novel cognitive model that can realize the bidirectional cognitive transformation between qualitative concepts and quantitative data based on probability statistics and fuzzy set theory [45]. As a response to the randomness of membership functions development by Zadeh [46] in 1965 [47], Li et al. [17,18] proposed the concept of the cloud model to reveal the relationship between uncertainty and certainty of many fuzzy concepts in the natural and social sciences. By establishing the normal cloud model,

the concept of uncertainty is transformed into explicit relations and data, and the inner relationship between randomness and fuzziness is revealed. The cloud model includes the forward and backward cloud transformation algorithms. The function of forward cloud transformation is to convert the qualitative concept (connotation) expressed by digital characteristic values into quantitative values (denotation), while the backward cloud transformation algorithm functions to convert the quantitative values expressed by concept denotation into the connotation of qualitative concepts expressed by digital characteristic values. The digital characteristic values include the expected value  $Ex$ , the entropy value  $En$ , and the hyper entropy value  $He$ , respectively. Let  $X$  be an ordinary set  $X = \{x_1, x_2, \dots, x_n\}$ , and let  $x$  be the sample. The specific steps of both algorithms are shown as follows. For the backward cloud transformation algorithm, the estimated value of expected  $Ex$  is calculated according to the sample data  $x_1, x_2, \dots, x_n$ , as shown in Equation (10):

$$Ex = \frac{1}{n} \sum_{k=1}^n x_k \quad (10)$$

Take  $m$  groups of samples randomly and reproducibly from  $X$ , and each group has  $r$  samples ( $m$  and  $r$  are positive integers;  $r$  is not necessarily equal to  $n$ ). Calculate the variance of each group of samples separately in Equation (11):

$$y_i^2 = \frac{1}{r-1} \sum_{j=1}^r (x_{ij} - Ex_i)^2, \quad i = 1, 2, \dots, m \quad (11)$$

where,  $Ex_i$  is the average within-group sample. According to the process of forward cloud transformation,  $y_1, y_2, \dots, y_m$  can be considered as a set of samples from the normal distribution  $N(En, He^2)$ . We then calculate the estimated values of  $En^2$  and  $He^2$  from the sample  $y_1^2, y_2^2, \dots, y_m^2$  as shown in Equations (12) and (13):

$$En^2 = \frac{1}{2} \sqrt{4(EY^2)^2 - 2DY^2}, \quad He^2 = EY^2 - En^2 \quad (12)$$

where,

$$DY^2 = \frac{1}{m-1} \sum_{i=1}^m (y_i^2 - EY^2)^2, \quad EY^2 = \frac{1}{m} \sum_{i=1}^m y_i^2 \quad (13)$$

For the forward cloud transformation algorithm, we first generate a normal random number  $y_i = R_N(En, He)$  with  $En$  as the expected value and  $He^2$  as the variance. Then we generate a normal random number  $x_i = R_N(Ex, y_i)$  with  $Ex$  as the expected value and  $y_i^2$  as the variance. Certainty ( $\mu(x_i)$ ) is then calculated according to Equation (14):

$$\mu(x_i) = \exp \left\{ -\frac{(x_i - Ex)^2}{2y_i^2} \right\} \quad (14)$$

We then get  $x_i$  with a certain degree  $\mu(x_i)$  as a cloud droplet and repeat the above steps to get  $n$  cloud droplets.

The cloud model is used to analyze the SPI index of the Haihe Plain to clarify the uniformity and stability of drought in this region.  $Ex$  reflects the center of gravity of the cloud drop in the cloud model diagram, and its value is the expectation of the SPI sample. The smaller the value of  $Ex$ , the stronger the drought in the area.  $En$  is the possible value range of the relative average deviation of SPI, which reflects the dispersion. The larger the  $En$ , the more uneven the distribution of cloud droplets and the more scattered the distribution of drought is.

The characteristic parameters of the cloud model are calculated based on the annual SPI of the 20 weather stations in the Haihe Plain and are assessed using bootstrapping. First, we randomly take 20 groups of samples, with 4 in each group. After 1000 iterations, the median of the calculation results is stable, and the final  $He$  and  $En$  are determined. The



normal cloud generator algorithm is used to draw a cloud map of the SPI membership degree according to  $Ex$ ,  $En$ ,  $He$ , and the number of cloud drops  $N_d$  ( $N_d = 1000$ ).

### 3. Results

#### 3.1. Precipitation Change

Figure 2 shows that the average precipitation in the Haihe Plain generally decreased gradually from the northeast to southwest. The average annual rainfall at the Chaoyang and Nangong stations is the smallest (<500 mm/year), and the average annual rainfall at the Miyun and Qinhuangdao stations is the largest (>640 mm/year).

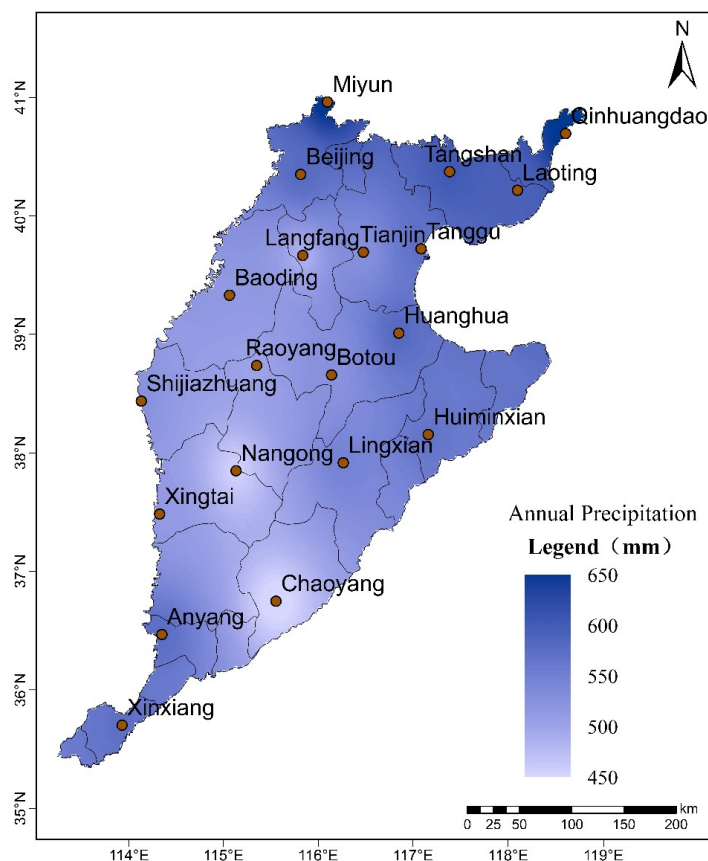


**Figure 2.** Spatial distribution of annual precipitation in the Haihe Plain. (ArcGIS10.2 was used to draw the spatial distribution map of the average annual precipitation of each station by inverse distance-weighted method).

#### 3.2. Drought Grade and Drought Frequency

Figure 3 shows different drought grades over different timescales. During the four seasons, the  $DF$  is highest in spring, and the most probable drought types are slight (19.0%) and moderate (15.9%). In summer, there is lower  $DF$  (<30%). The proportion of slight drought is 14.3%; however, severe drought increased (6.4%). Except for moderate drought, the  $DF$  of extreme drought, severe drought, and slight drought in autumn are almost similar to those in the summer. In winter, the  $DF$  of extreme drought is the smallest at 3.7%, while there is little difference among the  $DF$  of other grades. The  $DF$  in spring and WGP have the same characteristics, both of them have no extreme drought and the biggest  $DF$  of slight drought. The total of  $DF$  in summer and MGP is very close. The reason for these phenomena is that the main growth period of wheat is in spring, whereas that of maize is in summer. At the annual scale, the  $DF$  of slight drought (7.0%) is lower than that of other timescales, while the  $DF$  of severe drought is higher than that of other timescales (7.9%). To summarize, the  $DF$  in spring is the highest with slight and moderate droughts in the Haihe

Plain, while the frequency of severe and extreme droughts in summer, autumn, and winter has similar values. Compared with other timescales, the frequency of extreme drought is the highest in WGP.

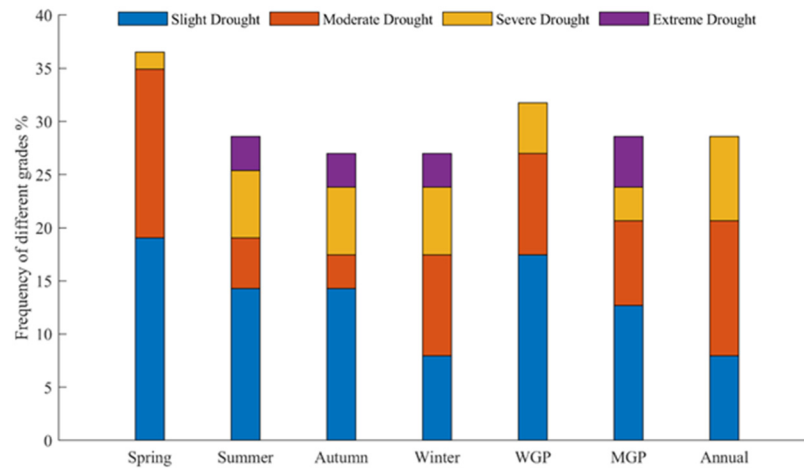


Figure 3. Frequency of drought occurrence in different timescales.

The spatial distribution of the frequency of different drought grades in the Haihe Plain is shown in Figure 4. The frequency range of extreme drought is under 1.6%, with the exception of around the Nangong station (frequency of 3.3%). The spatial distribution trend shows that the *DF* of the extreme grade of south is greater in the south than in the north, and the west is larger than the east. The *DF* interval of severe drought ranges mostly between 0.8 and 3.2%, with outliers at Leting (6.5%) and Botou (5.7%). The spatial trend shows that the *DF* at severe grade is larger in the east than in the west. The *DF* for moderate drought ranges from 0.8 to 8.1%, with larger values in the northwest and southernmost areas in comparison to the south-central region. Concerning slight drought, *DF* frequency ranges between 8 and 19%, and the overall trend of *DF* is increasing from the center to the surrounding areas, especially in Langfang (26.2%) and Tanggu (22.2%).

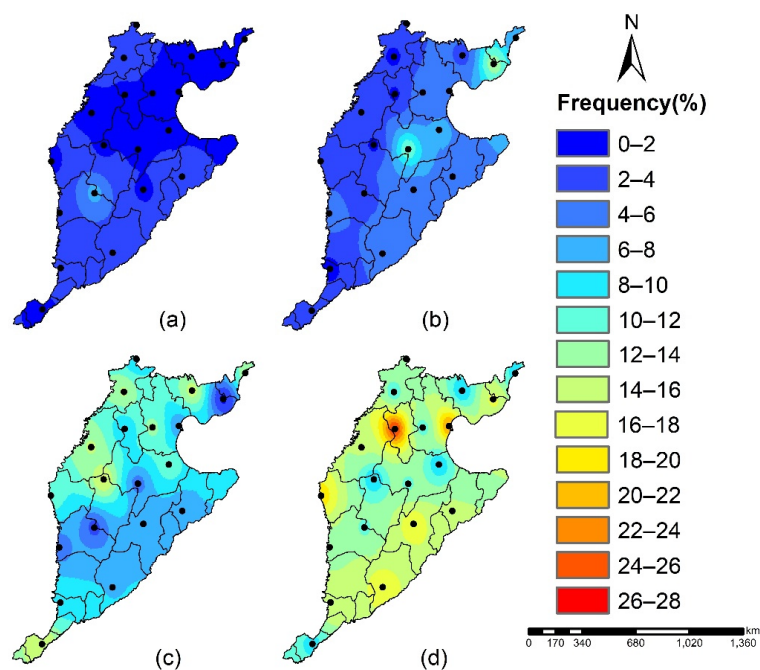
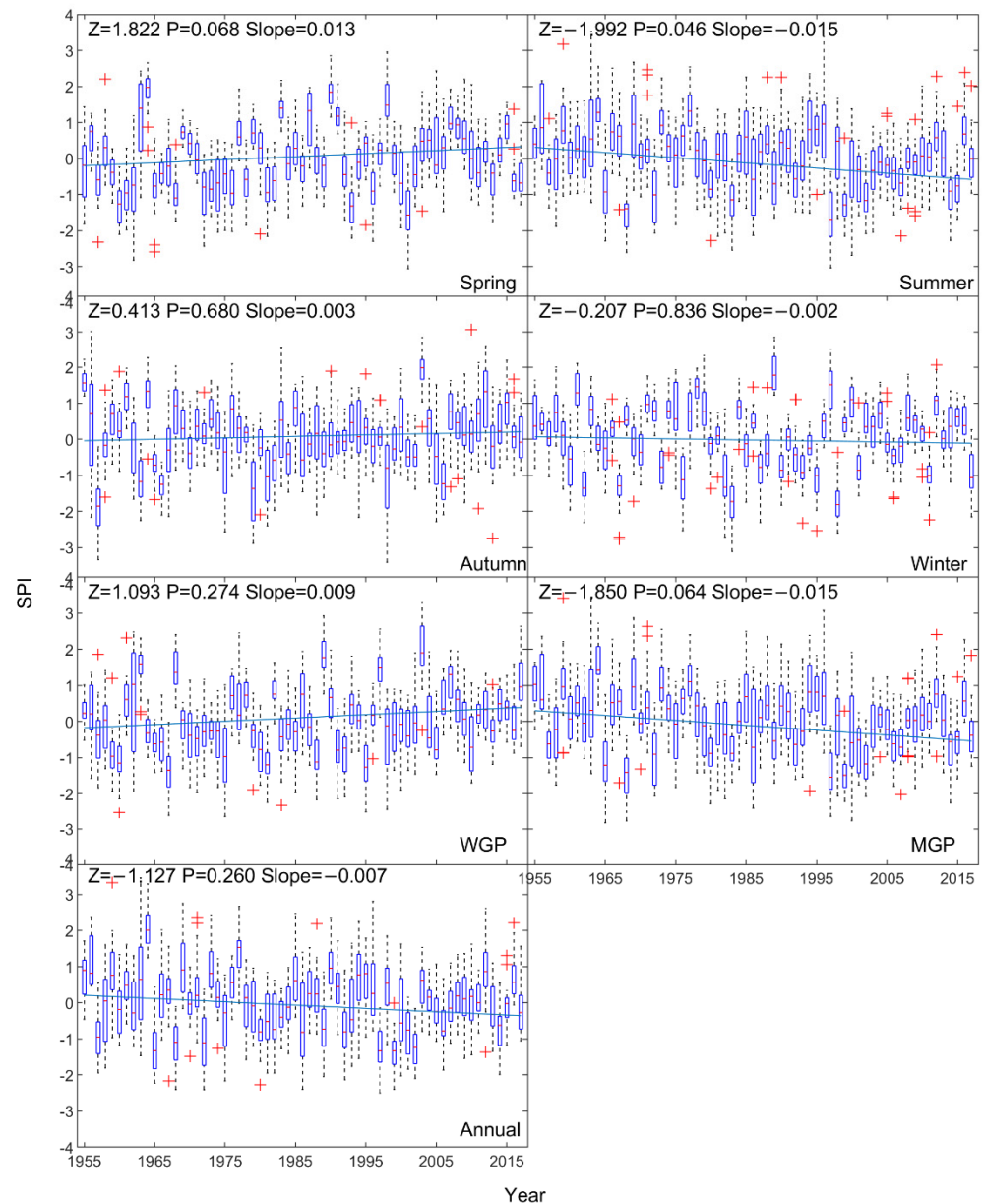


Figure 4. Spatial distribution of (a) extreme drought, (b) severe drought, (c) moderate drought, and (d) slight drought frequencies in the Haihe Plain, calculated by annual SPIs.



### 3.3. Characteristics of Drought Time Variation in Different Timescales

To analyze the characteristics and changing trends of SPIs at different timescales, we used boxplots to analyze the SPI change trend of the 20 weather stations (Figure 5). The trend line of the SPI by year was derived along with the  $Z$ ,  $p$  value, and Sen's slope by using the trend of the MK test. In Figure 5, the SPIs of 20 stations in each year constitute a single box. If the length of the box and whiskers is longer, this means that the SPIs of the corresponding year exhibit greater variability.



**Figure 5.** Boxplots of interannual SPI calculated for different time periods. For each box, the central mark indicates the median, and the bottom and top edges of the box indicate the 25th and 75th percentiles of 20 stations, respectively. The whiskers extend to the most extreme data points, and the outliers are plotted individually using the “+” symbol.

The mean value of the SPIs in spring is  $-1.341$ , which is the lowest of all the seasons. In other words, drought is most severe in spring. The differences of box length are large, which means the difference of SPI between stations and between years is large. The positive slope of the SPI trend line indicates a decreasing spring drought ( $Z = 1.822$ ,  $p = 0.068$ ). In

summer, the box length increases and there are many discrete points. In other words, there is a large difference between stations in each year. The SPI trend for summer indicates that the drought is increasing significantly ( $Z = -1.992$ ,  $p = 0.046$ ). The average value of the SPI in autumn is 0.008, which is the largest of the four seasons. The autumn box is the most concentrated of the four seasons. The autumn SPI trend line has a non-significant, near-zero slope. In winter, the box has higher inter-annual variability, but the trend line is the gentlest. For the two crops, SPI in WGP is close to and slightly smaller than that of spring. However, the boxplot of MGP is more discrete than that of summer; the SPI has a decreasing trend ( $p < 0.1$ ), which is slightly smaller than that of summer. At the annual timescale, the SPI shows a small decreasing trend, which indicates that the Haihe Plain is experiencing a dry trend. From 1955 to 2017, the SPI of the Haihe Plain showed a drought trend, the drought in spring tends to weaken, while the drought in summer tends to be serious and reaches a significant level.

#### 3.4. Spatial Variation Characteristics of Drought at Different Timescales

The years 1999 (dry year), 2015 (normal year), and 1977 (wet year) were selected as example years to analyze the distribution characteristics of different timescales and grades of drought (Figure 6). In the spring of 1999, there was a slight drought in the southern portion of the Haihe Plain, with a normal spatial pattern elsewhere. However, by the summer of 1999, the intensity and area of drought were extensive, with smaller areas of moderate, severe, and extreme drought. In the autumn of 1999, there was a slight, persistent, drought in the western area of the plain. In 2015, the area of slight drought was extensive and there were sporadic areas of severe drought. The year 1977 saw no drought, except for a small area of slight drought near the Xingtai, Anyang, and Xinxiang stations in summer as well as Xinxiang in winter. Summer was the season with the largest difference in the SPI during these three typical years. In winter, the difference of the SPI over the typical years is the smallest.

Drought in the growing season timescales exhibited slight differences from the climatological seasons. During the WGP in 1999, only a mild drought occurred in most of the western and southeastern border areas (near the Xingtai, Nangong, and Huiminxian stations), and no drought occurred in other typical years and areas. The degree of drought during MGP increased significantly. There were droughts of different grades in most regions in 1999 and for about half of the regions in 2015. In 1999, the drought grades were mainly moderate and severe, and the droughts in the north were more serious than those in the south. There were mainly slight and moderate droughts, which were concentrated in the south in 2015, near the Chaoyang station during the WGP. Most of the areas were near normal and the difference between droughts was smaller in 2015, as only a small area in the south experienced either a slight or moderate level of drought.

Overall, the distribution of drought grades and areas during the four seasons is prominently different across the 3 typical years and between regions. In a normal year, the spatial variation of SPI is small. In a wet year, the regional differences of the SPI are large, and SPI is larger in the north. In a dry year, the drought in the summer and the MGP is more severe, and the drought grade of the north is higher than that of the south. In other words, the north is drier in a dry year and wetter in a wet year. Among different seasons, the spatial variation of the SPI is the biggest in summer and the smallest in winter, and the drought grade distribution map of the annual scale is close to that of summer.

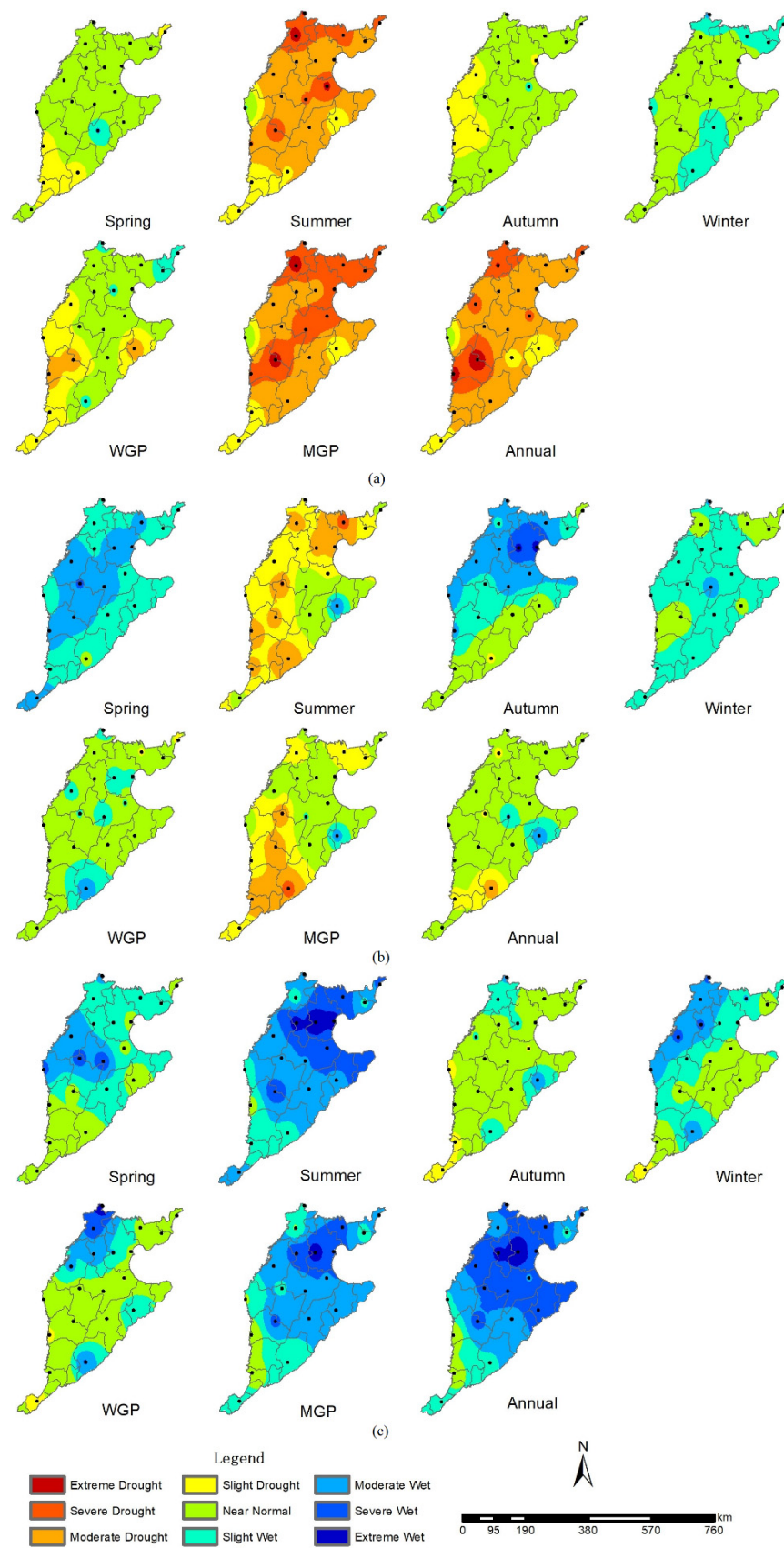


**Figure 6.** Spatial distribution of the SPI at different timescales in typical years. (a) 1999—dry year, (b) 2015—normal year, (c) 1977—wet year.

### 3.5. Spatiotemporal Variation Characteristics of Drought Based on Cloud Mode

In order to further analyze the stability and uniformity of the SPI, the characteristic values  $Ex$ ,  $En$ , and  $He$  of each station at different timescales were calculated by the multi-step backward cloud transformation based on sampling with replacement [48]. The cloud droplets were then calculated by the positive cloud generator algorithm to draw the membership degree of the SPI cloud (Figure 7).

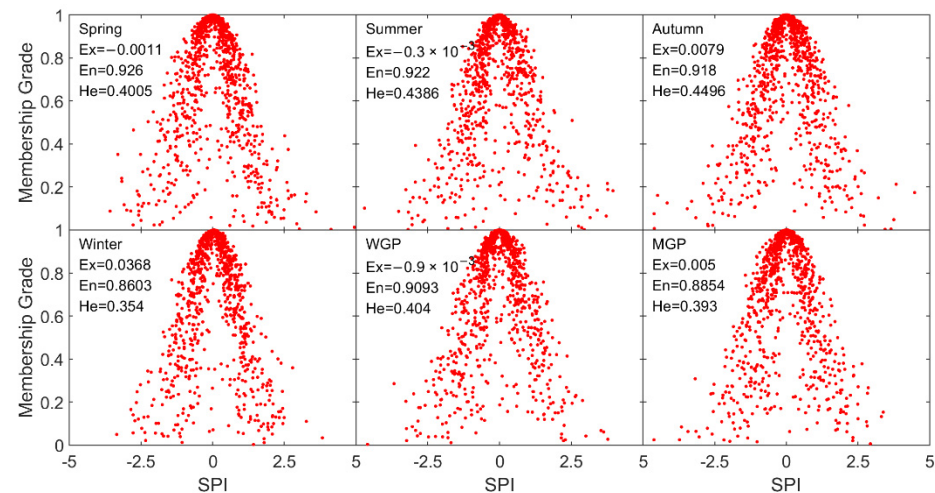


**Figure 7.** Cloud chart of the SPI membership degree at different timescales.

Figure 7 shows that in spring the  $Ex$  is the smallest ( $Ex = -0.0011$ ) and  $En$  is the biggest ( $En = 0.926$ ) at different timescales. That means the drought in spring is the most serious, and the variation range of SPIs is the widest. Summer and WGP are the next two timescales susceptible to drought because their  $Ex$  are both negative. The  $He$  (0.4496) in autumn is the biggest at different timescales, which means that the variation of membership grade for some certain SPI has the widest range, and the randomness is the largest. Meanwhile, the autumn has the thickest cloud layer in the cloud chart as the maximum of  $He$  in autumn, which indicates that the stability of the nonuniformity of the SPI distribution in autumn is the lowest. The winter entropy ( $En$ ) and super entropy ( $He$ ) are the smallest out of the four seasons, which shows that the SPI is the most stable and uniform in winter.

To analyze the homogeneity and stability of the SPI in different stations and different years, the SPI characteristics of each typical year and typical station were calculated, and a membership cloud chart was drawn. Figure 8 shows the cloud map of 1999, which is the driest year overall. The distribution of cloud droplets is relatively condensed to the left of the figure and the cloud layer is very thin, this indicates that the drought grades of each station are relatively concentrated in this year. Moreover, the distribution shows that the difference of the SPI between stations is small and the stability of the SPI is strong. In 2015, the cloud droplets were evenly distributed on both sides of “SPI = 0” and the cloud layer became thicker. The uniformity and stability of the distribution of the 2015 drought were lower than that of 1999 (dry year). In 1977, the cohesiveness of cloud droplets was the lowest of the three typical years, and the cloud droplets were more scattered and moved to the right of the figure; this indicates that the data of the SPI membership degree of each station in this year were more discrete, and the evenness and stability of drought occurrence were the lowest. In conclusion, the greater clustering towards the left side of the map indicates drier conditions; the more agglomerated the cloud droplets, the stronger stability of drought, and the smaller differences among regions.

Among the three stations, the distribution of cloud droplets at the Beijing station is the most dispersed (Figure 8). However, it has strong cohesiveness, a thick cloud layer, the smallest entropy ( $En = 0.856$ ), and the largest super entropy ( $He = 0.4988$ ). Therefore, the fuzziness and randomness of drought occurrence at the Beijing station are small, so



it is the most unstable. The cloud droplets of the Botou station exhibit the largest  $Ex$  and are more cohesive. The thickness of the cloud layer is significantly lower than that at the Beijing station, so the interannual drought period is concentrated with strong uniformity and stability. The entropy of the Chaoyang station is the largest, which shows that the membership degree of the SPI is the most fuzzy and random. Therefore, the smaller the SPI between stations, the more serious the drought; the higher the frequency of the drought, the more discrete the drought, and the lower the uniformity and stability of the drought. Compared to the typical annual cloud map, the cloud droplets of the typical station cloud map are more scattered, less cohesive, and thicker. Therefore, the difference of drought occurrence among the annual scales is greater than that among the stations in the Haihe Plain, and the interannual drought occurrence is more uneven and unstable.

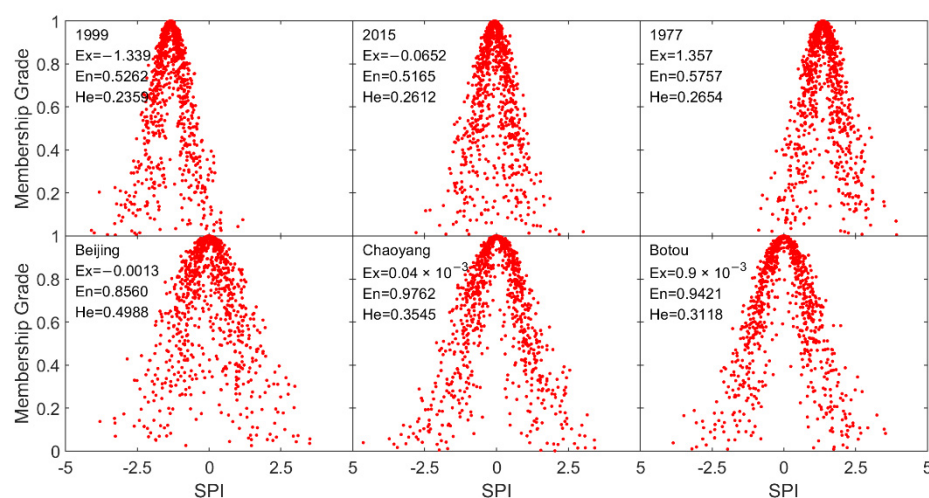


Figure 8. SPI membership cloud map of typical years and stations.

#### 4. Discussion

The Haihe Plain is a major agricultural area in Northern China and is part of the North China Plain and Haihe River Basin. This area has experienced serious water shortages over the last 30 years. Many scholars have studied drought in the Haihe River Basin, but few have studied drought in the Haihe Plain alone. Fan et al., calculated the standardized precipitation evaporation index of the Haihe River Basin and analyzed the temporal and spatial characteristics of drought in the area [31]. We found that the frequency of all drought grades in the Haihe River Basin is slightly lower than that of the Haihe Plain, as determined in this study. In addition, their results show that the frequency of spring drought is the highest in all seasons, followed by summer drought. These findings are consistent with the results of the present study. Our results show that the frequency range of drought occurrence is consistent with those of Zong et al. [49], who also analyzed the spatial and temporal distribution characteristics of drought in the Haihe River Basin using the SPI. Yan et al. [50] used a relative humidity index and a fuzzy set pair evaluation to determine the area and annual change of different drought grades in the Haihe River Basin, and the main frequency interval and area of drought occurrence in our study agree with their results. Wang et al. [51] revealed the spatial and temporal distribution characteristics of drought in the Haihe River Basin. They found that the droughts in the Haihe Basin featured spatial distribution characteristics of “high frequency, low intensity” and “low frequency, high intensity.” These characteristics are consistent with the results of our study; however, our results differ to Wang’s result in that the winter drought in the basin is the most serious and the summer drought is relatively low.

In this paper, the cloud model was used to analyze the uniformity and stability of the SPI on time scale and spatial scale in the Haihe Plain. In terms of the cloud model algorithm, this paper used the median value of multiple cycle results instead of the average when

calculating  $En$  and  $He$  with the multi-step reverse-reverse cloud transformation algorithm. It greatly reduced the probability of imaginary numbers in the calculation results and enhanced the stability of the quantized results. When comparing the cloud map of the SPI compared with that of the original precipitation, we found that the difference of each site SPI membership cloud image decreased. Because the SPI is the relative value derived from the rainfall, it also means that the calculating process of the SPI lost some randomness and stability of the precipitation information.

## 5. Conclusions

Drought occurs with an annual drought frequency of 28.6% in the Haihe Plain. The frequency of drought in spring is the highest across seven timescales, reaching 36.5%; it primarily occurs at grades of slight and moderate drought. However, the frequencies of severe and extreme drought in summer and autumn are higher. The MK trend analysis showed that the SPI of spring, autumn, and WGP have increasing tendencies, while those of summer, MGP, and annual showed decreasing trends; the decreasing trend reached a significant level ( $p = 0.046$ ) especially in summer. The Haihe Plain as a whole had a drying trend over the last 63 years. In terms of spatial distribution, the SPI in the northwest was the smallest and increased gradually toward the south; the distribution of drought varied in different hydrological years, and the severity of drought in dry year increased from southeast to northwest.

The results of the cloud model analysis using the annual SPI show that the drought characteristics in the Haihe Plain has not been significant over the past 63 years. The SPI randomness of each site decreased significantly and tended to be stable and uniform. The deterministic and stable SPI of each station were stronger in dry years, and the randomness and instability were stronger in wet years. Spatially, the higher the drought grade, the weaker the randomness of inter-annual SPI and the stronger the stability. In addition, the inter-annual differences of the characteristic values of the SPI cloud model were bigger than the differences among sites, and the inter-annual randomness and inhomogeneity of the SPI were higher.

Notably, only the characteristics of spatial and temporal drought in the Haihe Plain were discussed in this article. Further study related to the causes of drought and its effect on crops is needed to better formulate the strategy for agricultural water management in the future.

**Author Contributions:** Idea, X.Z. and Y.F.; methodology, X.Z. and D.W.; data processing, R.S. and Q.G.; writing—original draft preparation, Y.F., X.Z. and R.G.A.; writing—review and editing, all authors; visualization, R.S. and X.Z.; supervision, D.W.; funding acquisition, Y.F. and D.W. All authors have read and agreed to the published version of the manuscript.

**Funding:** This research was funded by Young Scientists Fund of the National Natural Science Foundation of China (No. 51609137) and National Key Research and Development Program of China (No. 2017YFC0405805-03). R.G.A. is supported by the U.S. Department of Agriculture, Agricultural Research Service (project number 2036-61000-018-000-D). USDA is an equal opportunity provider and employer.

**Data Availability Statement:** Data sharing not applicable. All analyses are based on publicly available meteorological data.

**Conflicts of Interest:** The authors declare no conflict of interest.

## References

1. McKee, T.B.; Doesken, N.J.; Kleist, J. The relationship of drought frequency and duration to time scales. In Proceedings of the 8th Conference on Applied Climatology, Anaheim, CA, USA, 17–22 January 1993; pp. 179–184.
2. Buttafuoco, G.; Caloiero, T.; Coscarelli, R. Analyses of drought events in Calabria (Southern Italy) using standardized precipitation index. *Agric. Water Manag.* **2015**, *29*, 557–573. [[CrossRef](#)]
3. Zhao, Y.; Guo, J.; Mao, K. Spatio-temporal distribution of typical natural disasters and grain disaster losses in China from 1949 to 2015. *Acta Geogr. Sin.* **2017**, *72*, 1261–1276. (In Chinese with English Abstract) [[CrossRef](#)]



4. Liu, S. *Strategies for Flood and Drought Disaster Control*; China Society Press: Beijing, China, 2016; Volume 1, p. 340. (In Chinese)
5. Yang, Y.; Fan, J.; Hu, Y.; Moiwo, J. Sustainability of Water-Use and Food Production in the Haihe Catchment. In *Sustainability in Food and Water: An Asian Perspective*; Sumi, A., Fukushi, K., Honda, R., Hassan, K.M., Eds.; Springer Netherlands: Dordrecht, The Netherlands, 2010; pp. 231–239.
6. Pedro-Monzonis, M.; Solera, A.; Ferrer, J.; Estrela, T.; Paredes-Arquiola, J. A review of water scarcity and drought indexes in water resources planning and management. *J. Hydrol.* **2015**, *527*, 482–493. [[CrossRef](#)]
7. Heddinghaus, T.R.; Sabol, P. A review of the palmer drought severity index and where do we go from here? In Proceedings of the 7th Conference on Applied Climatology, Salt Lake City, Utah, 10–13 September 1991; pp. 242–246.
8. Guttman, N.B.; Wallis, J.R.; Hosking, J.R.M. Spatial comparability of the palmer drought severity index. *J. Am. Water Resour. Assoc.* **1992**, *28*, 1111–1119. [[CrossRef](#)]
9. Vicente-Serrano, S.M.; Beguería, S.; López-Moreno, J.I. A multiscale drought index sensitive to global warming: The standardized precipitation evapotranspiration index. *J. Clim.* **2010**, *23*, 1696–1718. [[CrossRef](#)]
10. Vicente-Serrano, S.M.; Beguería, S.; López-Moreno, J.I.; Angulo, M.; Kenawy, A.E. A new global 0.5 gridded dataset (1901–2006) of a multiscale drought index: Comparison with current drought index datasets based on the Palmer Drought Severity Index. *J. Hydrometeorol.* **2010**, *11*, 1033–1043. [[CrossRef](#)]
11. Guttman, N.B. Comparing the palmer drought index and the standardized precipitation index. *J. Am. Water Resour. Assoc.* **1998**, *34*, 113–121. [[CrossRef](#)]
12. Hayes, M.J.; Svoboda, M.D.; Wilhite, A.D.; Vanyarkho, O.V. Monitoring the 1996 drought using the standardized precipitation index. *Bull. Am. Meteorol. Soc.* **1999**, *80*, 429–438. [[CrossRef](#)]
13. Lloyd-Hughes, B.; Saunders, M.A. A drought climatology for Europe. *Int. J. Climatol.* **2002**, *22*, 1571–1592. [[CrossRef](#)]
14. Feng, B.; Zhang, G.; Li, F. Characteristics of seasonal meteorological drought and risk regionalization in Songhua River Basin. *Sci. Geogr. Sin.* **2016**, *36*, 466–474. (In Chinese with English Abstract)
15. Zhi, P.; Wang, Y.; Shao, M.; Jia, X.; Li, X. Spatiotemporal analysis of multiscale drought characteristics across the Loess Plateau of China. *J. Hydrol.* **2016**, *534*, 281–299. [[CrossRef](#)]
16. Li, W.; Duan, L.; Wang, W.; Wu, Y.; Liu, T.; Quan, Q.; Chen, X.; Yin, H.; Zhou, Q. Spatiotemporal characteristics of drought in a semi-arid grassland over the past 56 years based on the Standardized Precipitation Index. *Meteorol. Atmos. Phys.* **2021**, *133*, 41–54. [[CrossRef](#)]
17. Li, D.; Meng, H.; Shi, X. Membership clouds and membership cloud generators. *Comput. Res. Dev.* **1995**, *32*, 15–20. (In Chinese with English Abstract)
18. Li, D.Y.; Liu, C.Y.; Gan, W.Y. A New Cognitive Model: Cloud Model. *Int. J. Intell. Syst.* **2009**, *24*, 357–375. [[CrossRef](#)]
19. Yan, Z.H.; Baetz, B.; Li, Z. A cloud-based dual-objective nonlinear programming model for irrigation water allocation in Northwest China. *J. Clean. Prod.* **2021**, *308*, 127330. [[CrossRef](#)]
20. Shan, B.Y.; Guo, S.S.; Wang, Y.Z.; Li, H.; Guo, P. Vine copula and cloud model-based programming approach for agricultural water allocation under uncertainty. *Stoch. Hydrol. Hydraul.* **2021**, *35*, 1895–1915. [[CrossRef](#)]
21. Zhang, H.Y.; Ji, P.; Wang, J.Q.; Chen, X.H. A Neutrosophic Normal Cloud and Its Application in Decision-Making. *Cogn. Comput.* **2016**, *8*, 649–669. [[CrossRef](#)]
22. Wang, J.Q.; Wang, P.; Wang, J.; Zhang, H.Y.; Chen, X.H. Atanassov's Interval-Valued Intuitionistic Linguistic Multicriteria Group Decision-Making Method Based on the Trapezium Cloud Model. *IEEE Trans. Fuzzy Syst.* **2015**, *23*, 542–554. [[CrossRef](#)]
23. Wang, J.Q.; Peng, J.J.; Zhang, H.Y.; Liu, T.; Chen, X.H. An Uncertain Linguistic Multi-criteria Group Decision-Making Method Based on a Cloud Model. *Group Decis. Negot.* **2015**, *24*, 171–192. [[CrossRef](#)]
24. Li, Y.; Chen, Y.Y. Variable precondition S-type cloud algorithm: Theory and application on water resources carrying capacity assessment. *Ecol. Indic.* **2021**, *121*, 107209. [[CrossRef](#)]
25. Yan, F.; Li, Z.J.; Dong, L.J.; Huang, R.; Cao, R.H.; Ge, J.; Xu, K.L. Cloud model-clustering analysis based evaluation for ventilation system of underground metal mine in alpine region. *J. Central South Univ.* **2021**, *28*, 796–815. [[CrossRef](#)]
26. Zhou, K.P.; Lin, Y.; Deng, H.W.; Li, J.L.; Liu, C.J. Prediction of rock burst classification using cloud model with entropy weight. *Trans. Nonferrous Met. Soc. China* **2016**, *26*, 1995–2002. [[CrossRef](#)]
27. Yin, C.; Qi, G.; Kang, Y. Analysis on characteristics of temporal-spatial potential evapotranspiration distribution in Gansu based on cloud model. *Trans. Chin. Soc. Agric. Eng.* **2015**, *31*, 152–158. (In Chinese with English Abstract)
28. Cheng, C.; Liu, Y.; Xing, J. Analysis of distribution characteristic of drought in Sichuan hilly area based on drought index and cloud model. *Yangtze River* **2015**, *46*, 1–5. (In Chinese with English Abstract)
29. Long, Y.; Liang, C.; Jing, N. Analysis on characteristics of temporal-spatial drought distribution based on cloud model and relative moisture index. *J. Irrig. Drain.* **2015**, *34*, 67–71. (In Chinese with English Abstract)
30. Jin, J.; Li, H.; Li, J. Analysis of characteristics of temporal-spatial drought distribution in Anhui Province based on cloud Model. *Water Resour. Power* **2017**, *35*, 1–5. (In Chinese with English Abstract)
31. Fan, Q.; Zhao, A.; Zhang, A. Characteristics of spatiotemporal variation of drought in the Haihe River Basin from 1965 to 2015. *Res. Agric. Mod.* **2019**, *40*, 507–517. [[CrossRef](#)]
32. WMO. *Standardized Precipitation Index User Guide* (Svoboda, M., Hayes, M. and Wood, D.); WMO: Geneva, Switzerland, 2012.
33. Kumer, M.N.; Murthy, C.S.; Sai, M.V.R.S.; Poy, P.S. On the use of Standardized Precipitation Index (SPI) for drought intensity assessment. *Meteorol. Appl.* **2009**, *16*, 381–389. [[CrossRef](#)]

34. Hong, W.; Svoboda, M.; Hayes, M.J.; Wilhite, D.A.; Wen, F. Appropriate application of the standardized precipitation index in arid locations and dry seasons. *Int. J. Climatol.* **2010**, *27*, 65–79.
35. Zhang, C.; Liu, H.; Song, Y. *Grades of Meteorological Drought*; AQSIQ; SAC: Beijing, China, 2017. (In Chinese)
36. Sun, X.; Wilcox, B.P.; Zou, C.B. Evapotranspiration partitioning in dryland ecosystems: A global meta-analysis of in situ studies. *J. Hydrol.* **2019**, *576*, 123–136. [[CrossRef](#)]
37. Hamed, K.H.; Rao, A.R. A modified Mann-Kendall trend test for autocorrelated data. *J. Hydrol.* **1998**, *204*, 182–196. [[CrossRef](#)]
38. Ashraf, M.S.; Ahmad, I.; Khan, N.M.; Zhang, F.; Bilal, A.; Guo, J. Streamflow Variations in Monthly, Seasonal, Annual and Extreme Values Using Mann-Kendall, Spearman's Rho and Innovative Trend Analysis. *Water Resour. Manag.* **2021**, *35*, 243–261. [[CrossRef](#)]
39. Agbo, E.P.; Ekpo, C.M.; Edet, C.O. Analysis of the effects of meteorological parameters on radio refractivity, equivalent potential temperature and field strength via Mann-Kendall test. *Theor. Appl. Climatol.* **2021**, *143*, 1437–1456. [[CrossRef](#)]
40. Alsafadi, K.; Mohammed, S.; Ayugi, B.; Sharaf, M.; Harsányi, E. Spatial–Temporal Evolution of Drought Characteristics Over Hungary Between 1961 and 2010. *Pure Appl. Geophys.* **2020**, *177*, 3961–3978. [[CrossRef](#)]
41. Kalisa, W.; Zhang, J.; Igbawua, T.; Ujoh, F.; Ebohon, O.J.; Namugize, J.N.; Yao, F. Spatio-temporal analysis of drought and return periods over the East African region using Standardized Precipitation Index from 1920 to 2016. *Agric. Water Manag.* **2020**, *237*, 106195. [[CrossRef](#)]
42. Lin, H.; Wang, J.; Li, F.; Xie, Y.; Jiang, C.; Sun, L. Drought Trends and the Extreme Drought Frequency and Characteristics under Climate Change Based on SPI and HI in the Upper and Middle Reaches of the Huai River Basin, China. *Water* **2020**, *12*, 1100. [[CrossRef](#)]
43. Sen, P.K. Estimates of the regression coefficient based on Kendall's tau. *J. Am. Stat. Assoc.* **1968**, *63*, 1379–1389. [[CrossRef](#)]
44. Burkey, J. A Non-Parametric Monotonic Trend Test Computing Mann-Kendall Tau, Tau-b, and Sen'Slope Written in Mathworks-MATLAB Implemented Using Matrix rotations. King County, Department of Natural Resources and Parks, Science and Technical Services section: Seattle, WA, USA. Available online: <http://www.mathworks.com/matlabcentral/fileexchange/authors/23983> (accessed on 27 August 2020).
45. Wang, G.; Xu, C.; Li, D. Generic normal cloud model. *Inf. Sci.* **2014**, *280*, 1–15. [[CrossRef](#)]
46. Zadeh, L.A. Probability measures of Fuzzy events. *J. Math. Anal. Appl.* **1968**, *23*, 421–427. [[CrossRef](#)]
47. Zadeh, L.A. Fuzzy sets. *Inf. Control.* **1965**, *8*, 338–353. [[CrossRef](#)]
48. Xu, C.; Wang, G.; Zhang, Q. A New Multi-Step Backward Cloud Transformation Algorithm Based on Normal Cloud Model. *Fundam. Inform.* **2014**, *133*, 55–85. [[CrossRef](#)]
49. Zong, Y.; Wang, Y.; Zhai, J. Spatial and temporal characteristics of meteorological drought in the Haihe river basin based on standardized precipitation index. *J. Arid. Land Resour. Environ.* **2013**, *27*, 198–202. (In Chinese with English Abstract)
50. Yan, D.; Yuan, Z.; Yang, Z. Spatial and temporal changes in drought since 1961 in Haihe River basin. *Adv. Water Sci.* **2013**, *24*, 34–41. [[CrossRef](#)]
51. Wang, W.; Yan, J.; Liu, Y. Characteristics of droughts in the Haihe Basin based on meteorological drought composite index. *Arid. Land Geogr.* **2016**, *39*, 336–344. [[CrossRef](#)]